Topology of the Flow Structures Behind an Inclined Projectile: Part B

K. C. Ward* and J. Katz†
Johns Hopkins University, Baltimore, Maryland

A series of flow-visualization experiments, aimed at resolving the flow structure in the lee of an inclined 3.5*l*/*D* ogive nose cone, was performed in a large towing tank. The observations consist of illuminating a thin slice of the flowfield with a laser sheet while distributing fluorescing dye in the water. The results of this study are presented as a series of closely spaced topology plots. They demonstrate that at $Re_D = 2.7 \times 10^5$ the lee flow structure is asymmetric throughout the model, and is dominated by continuously generated, multiple, large-scale flow structures. Their development and interaction are described in detail. Phenomena such as entrainment of one center of coalescing stream surfaces by another one, as well as the appearance of a new pair of secondary structures, occur several times along the model. The "complete detachment" of a focus from the model's surface is also demonstrated. This paper contains also several surface pressure distributions, and an attempt, with partial success, is made to compare them to the crossflow topologies.

Introduction

THE development of asymmetric flow structures in the lee of inclined bodies of revolution and the resulting side forces were subjects of extensive research for the past thirty years.[1-10] The experimental research activities have included primarily force and surface pressure measurements,[2-4] flow visualization[5-8] and partial mapping of the velocity field utilizing pitot tubes,[6] and laser Doppler velocimetry.[9,10] Both theoretical and numerical studies were performed[11,12] and several extensive review papers were also written.[13,14] In summary, these studies have demonstrated that when a body of revolution is inclined to the freestream, its boundary layer separates and a complex flow structure forms on its lee side. When the incidence angle is increased beyond a critical value (twice the half-apex angle for bodies with a sharp nose cone[2]) and above a certain Reynolds number (in the order of 1×10^5, based on the base diameter D), the lee flow becomes asymmetric. Attempts to plot the resulting crossflow topology were made by Wardlaw and Yanta,[10] Tobak and Peake,[15] and by the present authors.[16] The latter[16] were sketched based on qualitative flow-visualization experiments in a towing tank utilizing laser-induced fluorescence. The model tested was a 3.5*l*/*D* ogive nose cone with a 10-in. base diameter and a sharp tip. This study has provided a series of vivid and detailed images of the crossflow structures at prescribed locations. It has also demonstrated the role of the Reynolds number and the incidence angle, in the formations of centers (or foci) of coalescing stream surfaces, as well as their development and interaction behind the model.

The initial series of flow-visualization experiments[16] have focused primarily on the large-scale structures in several axial sections, spaced every $X/D = 0.5$ (X being the axial distance and D the base diameter). Based on these observations, and due to the realization that the initial spacing has been too large, the present study presents the results of a more detailed series of observations, at a single incidence angle of 45 deg and Reynolds number of 2.7×10^5. The primary focus is on the generation of new secondary flow structures, their growth and migration, and their interaction with neighboring "older" foci and saddle points. The results of these observations are presented as a series of sketched crossflow topologies. An attempt is also made to reconstruct a three-dimensional image of the flow structures in the lee of the model by combining some of the individual topologies. Finally, the results of surface pressure distributions measurements at selected cross sections are also presented. A discussion and a comparison of these distributions to the observed flow structure follows.

As is evident from this introduction, the present paper is a direct continuation of our original study,[16] which also contains a detailed description of the test facility. A brief description of the experimental setup is provided also in Part A of this paper.[17] The description of the pressure measurement system is a little more detailed here, since it was not included in Ref. 16.

Experimental Setup

A short description of the flow-visualization setup was already presented in Part A of this paper.[17] The flow-visualization experiments were performed by illuminating a thin slice (1 mm thick) of the flowfield with an argon-ion laser while seeding the water with Rhodamine 6G, a fluorescing dye, prior to each run. The optical system was set to illuminate a vertical plane, which is perpendicular to the direction of motion. The flow-visualization images were recorded with a submerged video system trailing about 10 ft behind the model. Each flow condition (incidence angle and location) was studied several times to insure repeatability. The water in the facility was allowed to settle for about 1 h between runs, and in some cases, as will be discussed later, the layover between runs was extended to 12 h. Our experience has indicated that for most cases, the layover of 1 h was sufficient to insure repeatability and to reduce the freestream turbulence to immeasurable levels. Part A of this paper[17] contains a discussion concerning the interpretaton of the observed images. This discussion leads to the conclusion that the observed flow "patterns" are actually the intersection of three-dimensional stream surfaces with the illuminated plane.

The surface pressure measurements were performed with a scanning valve, controlled by a PC-based data acquisition system. The velocity (measured with a submerged pitot tube) was held constant at 3.4 ft/s. Because of the resulting low pressures (variations in the order of ± 0.2 psi), a sensitive transducer (0.5 psi peak to peak with a 0.1% accuracy) was installed in the scanning valve. The low pressures also required repeated calibration before and after each run. The reference

Received Sept. 6, 1988; revision received April 7, 1989.

*Research Engineer, Department of Mechanical Engineering: currently Design Engineering Supervisor at Recreonics, Indianapolis, IN.
†Assistant Professor, Department of Mechanical Engineering.

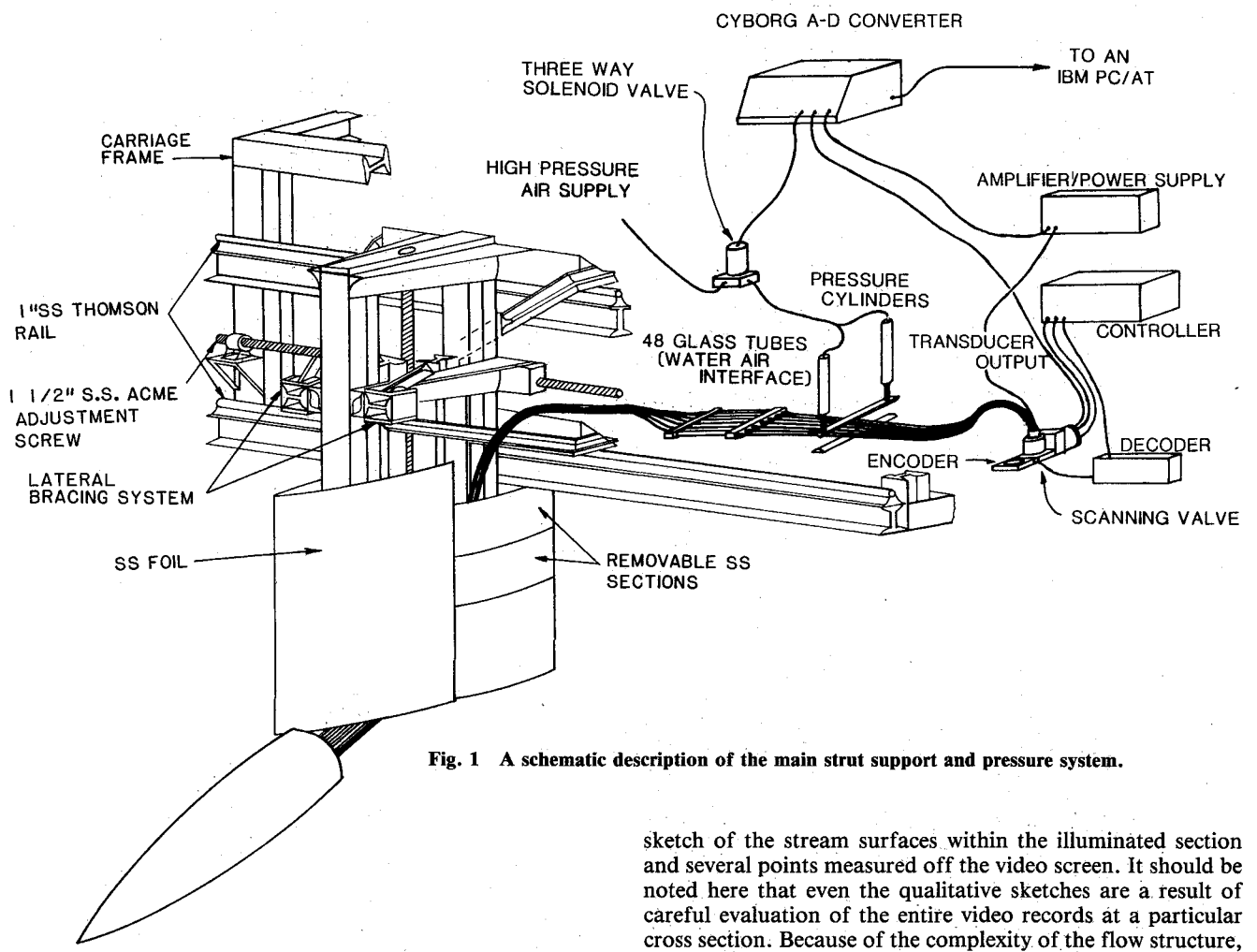

Fig. 1 A schematic description of the main strut support and pressure system.

level was a glass tube containing water at elevations different from the tank's surface level. The primary difficulty was the elimination of small bubbles within the tubes connecting the taps to the transducer. As shown in Fig. 1, each pressure tap was connected to a horizontal capillary glass tube, with a 1/32 in. internal diameter, which was positioned normal to the direction of motion. An air-water interface was maintained within these glass tubes, and the lines leading to the valve contained only air. The velocity chosen for these experiments was the highest allowing a complete cycle of the scanning valve (operating at two samples per second) during one uninterrupted run of the carriage. Each run was repeated four times, and the averaged data, as well as the highest and lowest results, are presented for each location. An evaluation of the error, based on the calibration curve and repeated measurments of the same reference level, was estimated to be 0.005 psi. This value corresponds to a maximum error of 0.07 in the values of C_p defined as $(P-P_{ref})/(0.5\rho V^2)$. P_{ref} is the static pressure of the pitot tube (compensated for the differences in elevation), and V is the carriage velocity. More detailed information about this setup is proved by Bueno-Galdo and Katz.[18]

Results

Flow Visualization

Sample photographs of the symmetric lee flow structure at a low Reynolds number, and topology plots of this particular flow, were presented in Ref. 17. The present study focuses on a higher Reynolds number, when the lee flow structure becomes asymmetric.

A series of crossflow topologies of $Re_D = 2.7 \times 10^5$ are presented in Fig. 2. Each image is a composition of a qualitative sketch of the stream surfaces within the illuminated section and several points measured off the video screen. It should be noted here that even the qualitative sketches are a result of careful evaluation of the entire video records at a particular cross section. Because of the complexity of the flow structure, it is quite difficult to find a single video frame containing a clear image of all of the secondary flow structures. As a result, determination of the data in each topology plot requires repeated careful examination of the entire set of records. In order to demonstrate this point, we examined the photographs, all of them at $X/D = 1.0$, shown in Fig. 3. The corresponding topology is presented at a higher magnification in Fig. 4. Point S1, as well as the structures with centers N1, N2, N3, and N4, are evident from Fig. 3a. The separation point S1, the structures defined by N1 and N2, as well as the location of surface saddle point X1 are visible in Fig. 3b. The existence of three distinct structures N5, N6, and N7 is demonstrated in Fig. 3c. A clear definition of the point X3, the small structure to its left, as well as a faded definition of X2, are presented in Fig. 3d. The location of X2, X3, and X4, as well as one of the stream surfaces entrained into the node "N7," are defined in Fig. 3e. X3 and the space between X2 and X3 are visible in Fig. 3f. The location of X5 is clearly visible in Fig. 3g, and a clearer evidence of the structure N7 is provided in Fig. 3h. The latter also shows traces of S2, whose location becomes clearly evident in Fig. 3i. The location of X6 is demonstrated in Fig. 3j. This set identifies all of the major structures of $X/D = 1$. The actual sketching of each topology requires repeated examination of all of the data as well as cross checking between different video frames and separate runs. An additional set of photographs at different cross sections is presented in Fig. 5.

The detailed observations were performed at every $X/D = 0.1$, starting from $X/D = 0.3$ up to $X/D = 3.0$ (some have been omitted in this paper since they do not contribute to the general picture). The flow at $X/D = 0.1$ was also examined, and a sample photograph at this section has already been presented in Ref. 16. Two primary facts become clearly evident from the topology sketches presented in Fig. 2. First,

under the current test conditions, the flow structure in the lee of the model is asymmetric over the entire length of the body. Second, this flow is dominated by continuously generated, multiple secondary flow structures. Even the first topology, at $X/D=0.3$, contains more secondary centers (foci or nodes) than the symmetric flow described in Part A of this paper.[17] The judgement of what structure is "primary" and what is "secondary" is obviously subjective, particularly when some structures appear to be quite small in upstream sections, and then grow further downstream. We have opted to define a certain structure as secondary when its effect on the overall picture, as well as its size, in a particular section, is small.

The evolution of the existing structures, as well as the formation of newer ones, can be identified by following the sequence of sketches shown in Fig. 2. As is evident from this series, between $X/D=0.3$ and 0.6, the upper left node lifts

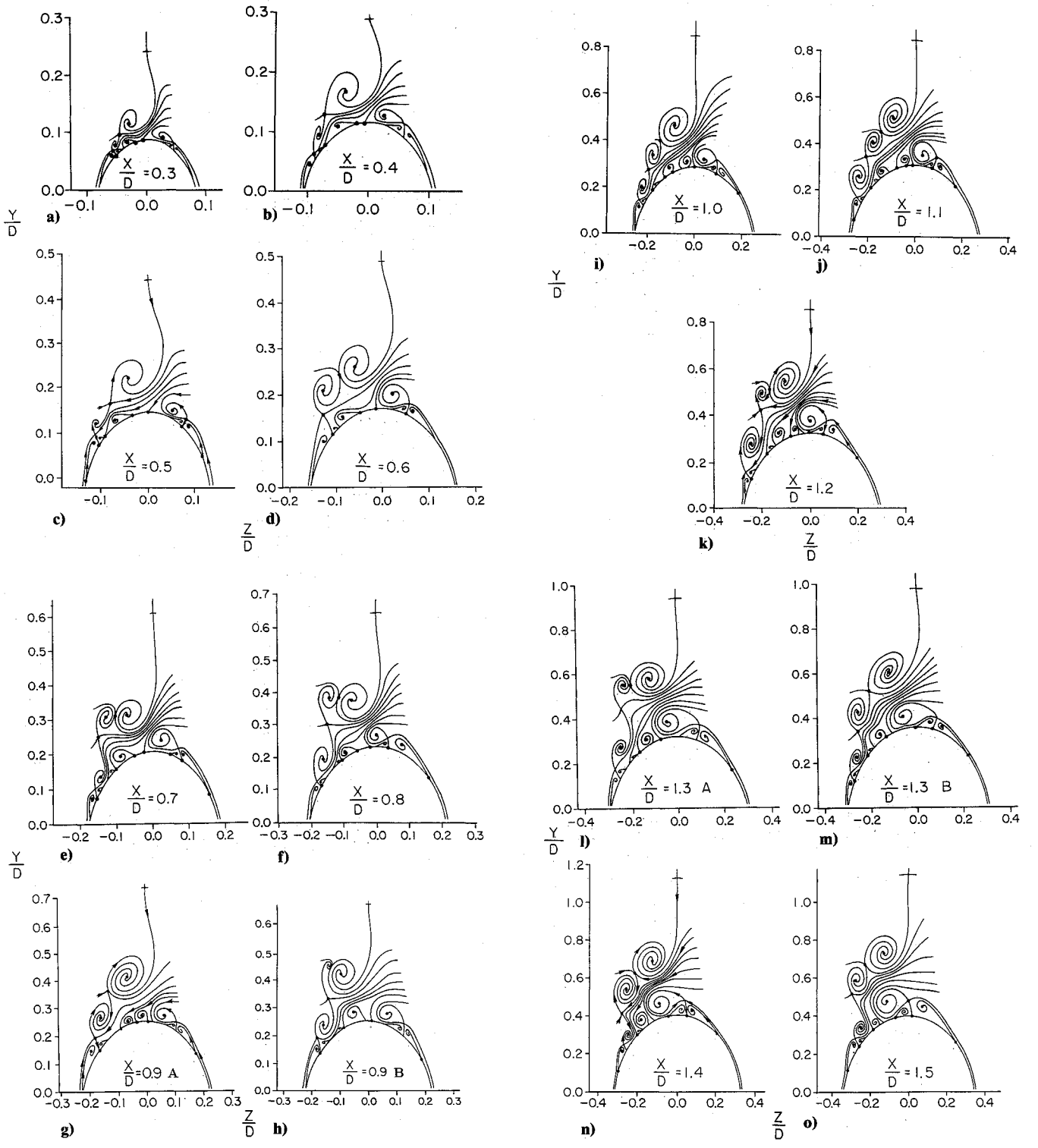

Fig. 2 Topology plots of the lee flow structures around a $3.5l/D$ tangent ogive at an incidence angle of 45 deg and $Re_D = 2.7\times10^5$ (● —indicates points measured on a video screen): a) $X/D=0.3$; b) $X/D=0.4$; c) $X/D=0.5$; d) $X/D=0.6$; e) $X/D=0.7$; f) $X/D=0.8$; g) $X/D=0.9$; h) $X/D=0.9$; i) $X/D=1.0$; j) $X/D=1.1$; k) $X/D=1.2$; l) $X/D=1.3$; m) $X/D=1.3$; n) $X/D=1.4$; o) $X/D=1.5$. (continued)

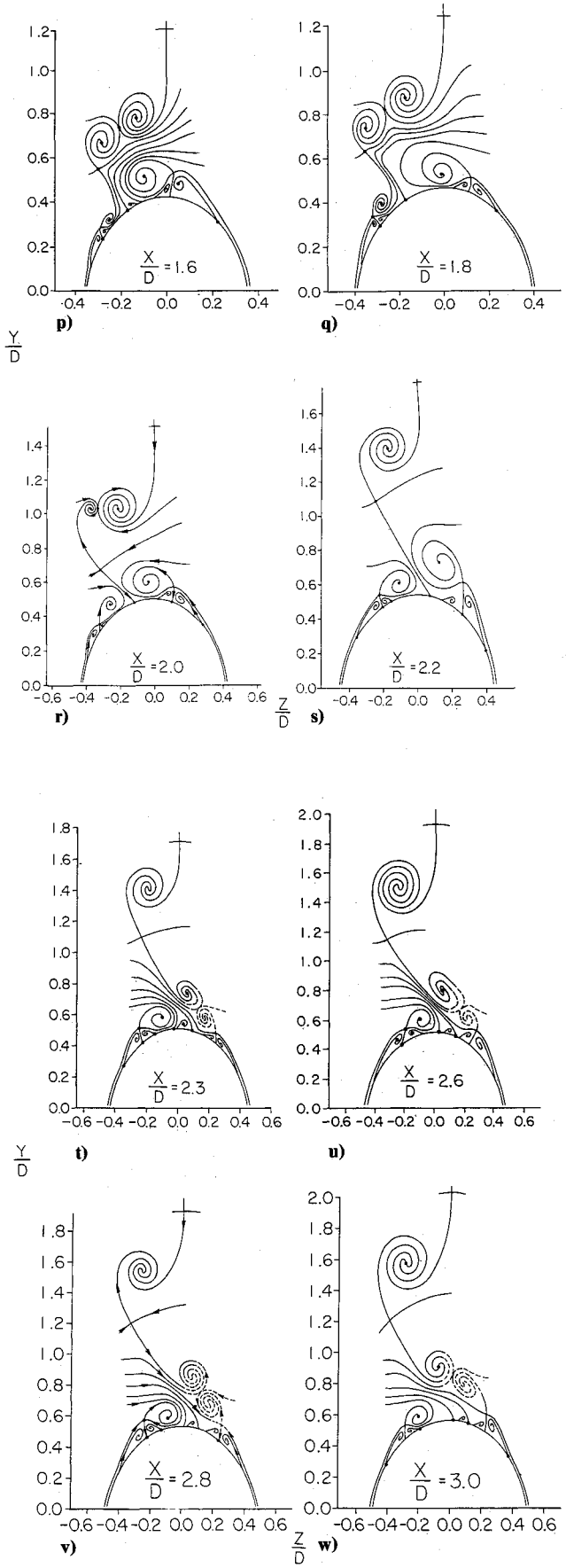

Fig. 2 (continued) Topology plots of the lee flow structures around a 3.5l/D tangent ogive at an incidence angle of 45 deg and $Re_D = 2.7 \times 10^5$ (● —indicates points measured on a video screen): p) $X/D = 1.6$; q) $X/D = 1.8$; r) $X/D = 2.0$; s) $X/D = 2.2$; t) $X/D = 2.3$; u) $X/D = 2.6$; v) $X/D = 2.8$; and w) $X/D = 3.0$.

away from the surface, the primary right focus moves towards the leeward meridian, and one of the left-side secondary structures increases in its size. This process is also demonstrated by several sample photographs in Fig. 5. As a result, at $X/D = 0.6$, there are two large foci on the left-hand side of the model, both containing fluid rotating in the same direction. Between $X/D = 0.6$ and 0.9, the lower focus is swept around the upper center while its "size" (here the "size" refers to its characteristic radius, namely, to the distance between the focus of the structure and the saddle point to the right of this focus) starts decreasing. Its identification at $X/D = 0.9$ is quite difficult, and its existence seems to depend on the free stream turbulence level. As a result, we have opted to present two flow topologies for $X/D = 0.9$. If the experiments are performed in very calm water (after about 12 h of recess between runs), the smaller center of coalescing stream surfaces is still evident to the left of the primary structure. If the experiments are performed after about 1 h of delay between runs, this small focus is no longer visible. A similar pair is also presented for $X/D = 1.3$. It should be emphasized here again that the freestream turbulence levels in both cases (1 and 12 h delays) are so low that they cannot be measured with velocity sensors (a hot film, for example). Note that between $X/D = 0.6$ and 0.9, an additional counterclockwise rotating structure starts growing while lifting away from the surface (shown also in Fig. 5), and a new pair of secondary structures form on the left-hand side of the model (compare the topologies at $X/D = 0.6$ and 0.7). An additional newly generated pair is also visible at $X/D = 1.0$.

As the structures containing clockwise-rotating fluid lift away from the surface, they leave under them a series of closely spaced nodes with fluid rotating in the counterclockwise direction. Several photographs demonstrating the existence of these closely spaced, multiple secondary structures are presented in some of the photographs of $X/D = 1.0$, as well as the sample image at $X/D = 1.7$ (Fig. 5). These nodes exist separately up to about $X/D = 1.3$, which is the first section displaying signs of the entrainment of a counterclockwise rotating secondary node by the original right primary center.

Before proceeding, we focus briefly on the topologies at $X/D = 0.5$ and 1.0, which represent the spacing between the sections of our original study.[16] Compared to the sketch of $X/D = 0.5$, the image of $X/D = 1.0$ contains one more clockwise-rotating center of coalescing stream surfaces. In the absence of an intermediate stage, we originally concluded, mistakenly, that the primary center of $X/D = 0.5$ splits into two structures at $X/D = 1.0$. We had no method of realizing that actually there are continuously generated new nodes, and that what appears as a small secondary node at a certain section becomes a major large-scale center farther downstream. Actually, one of the structures at $X/D = 0.5$ is already completely entrained into the large upper center at $X/D = 1.0$. Note that the lowest left-hand secondary structure of $X/D = 0.5$ actually appears as a major center at $X/D = 1.0$ (its focus is located at $Y/D = 0.37$). Furthermore, at a lower Reynolds number, the visible traces of asymmetry in the flow geometry start farther downstream.[16] As a result, the topology at $X/D = 1.0$ and $Re_D < 2.7 \times 10^5$ should resemble the current sketches of $X/D = 0.9$ or less. This statement is clearly substantiated by Ref. 16, which contains a series of photographs at the same location, but at different Reynolds numbers.

The entrainment of one center of coalescing stream surfaces by another repeats itself between $X/D = 1.3$ and 1.4 and then again between $X/D = 2.0$ and 2.2. Sample photographs of the flow between $X/D = 1.5$ and 2.0 are also presented in Fig. 5. Thus, three cycles are completed along the model, each consisting of the growth of a secondary structure while lifting away from the surface, its rotation around the original left primary focus, and then its eventual entrainment. The third cycle also involves an additional phenomenon, namely, the "complete detachment" of the original primary focus. In

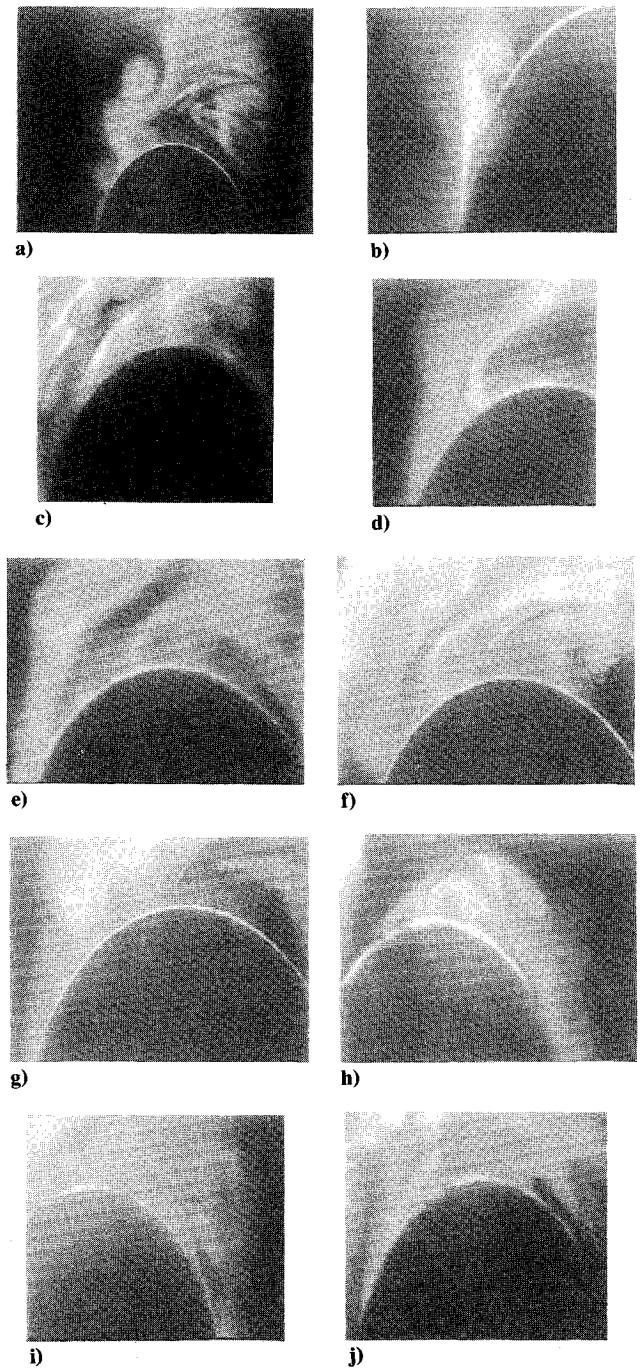

Fig. 3 A series of sample photographs of the flow structure at $X/D = 1.0$ and $Re_D = 2.7 \times 10^5$. This set demonstrates how the topology at this section has been plotted.

order to explain the term complete detachment, we compare the topologies at $X/D = 1.5$ to 2.0. The primary difference between these sketches occurs below the two upper centers that interact with each other. Note that at $X/D = 1.5$, the saddle point located at $Y/D = 0.5$ is connected to the focus of the structure below it, whereas at $X/D = 2.0$, the same saddle point is connected directly to a surface saddle point. This subtle change creates a clear stream surface which prevents the fluid arriving from the right-hand side of the model from reaching the left secondary structures. If one ignores for a brief moment the upper two structures, the topology below is a "warped" sketch of the symmetric flow shown in Ref. 17. Beyond this stage, a mirror image of the processes occurring upstream starts occurring on the right-hand side of the model. The initial stages of detachment of the right primary center can be observed up to $X/D = 3.0$. Unfortunately, this is the

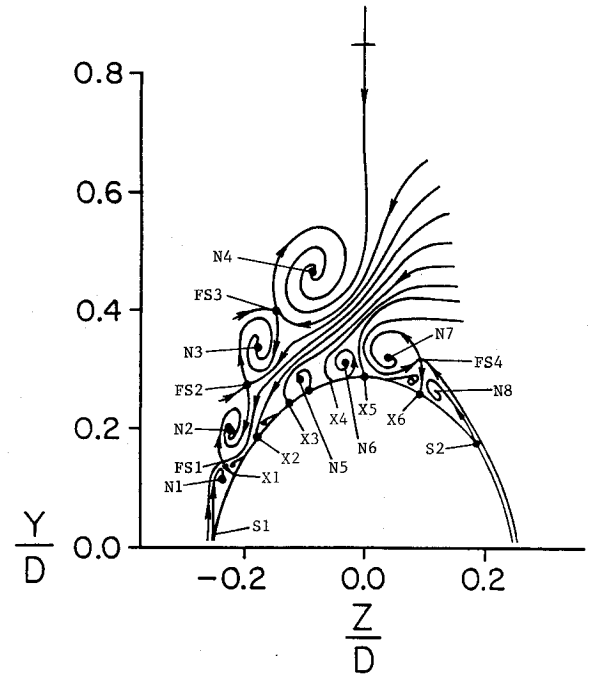

Fig. 4 A topology of the lee flow structure at $X/D = 1.0$.

end of our model. Note also that beyond $X/D = 1.6$, the two interlacing upper structures exist in a separate shell, and are no longer entraining fluid originating from the model's boundary layer. This state is defined in the present paper as a complete detachment.

Because of the difficulties in visualizing the evolution of the lee flow structures in our minds, an attempt was also made to draw a three-dimensional sketch of this flow. The results are presented in Fig. 6. They combine several topology sketches and additional lines connecting corresponding saddle points and foci. Some of the stream surfaces were removed for clarification.

Surface Pressure Measurements

The pressure distributions at three sections, $X/D = 0.9$, 1.9, and 2.9, and at two different incidence angles, 35 and 45 deg, are presented in Fig. 7. It should be noted here that the present Reynolds number, 2.7×10^5, was found by Lamont[19] to be the boundary between laminar and transitional flows, for both incidence angles. The terms "laminar," "transitional," or "turbulent" refer to the boundary layer on the surface of the model. The sensitivity of this flow to changes in the Reynolds number, the freestream turbulence level, and even the roll angle (Refs. 3, 4, 10, 16, and 19, for example) make any comparison between the present pressure distributions and other measurements quite difficult. We do not know of any measurements exactly at the same conditions as in the present study. Some discussion will follow.

The present results for 35 deg confirm what has already been demonstrated in Ref. 16, namely, that the flow remains almost symmetric at 35-deg incidence and resembles the images shown in Part A of this paper.[17] In fact, only a slight lifitng of the left primary center occurs at the presently selected Reynolds number. During our previous study,[16] this asymmetry was detected first at high X/D, and with increasing Reynolds numbers has propagated upstream. These observations are substantiated by the current pressure measurements. At $X/D = 0.9$, the pressure minima and inflection points are located symmetrically relative to the leeward meridian. Recovery of the pressure on the right-hand side occurs at a higher lateral angle, probably due to the closer proximity of the right primary structure to the surface. The two distributions farther downstream ($X/D = 1.9$ and 2.9) are quite similar, both displaying the existence of a secondary pressure minimum close

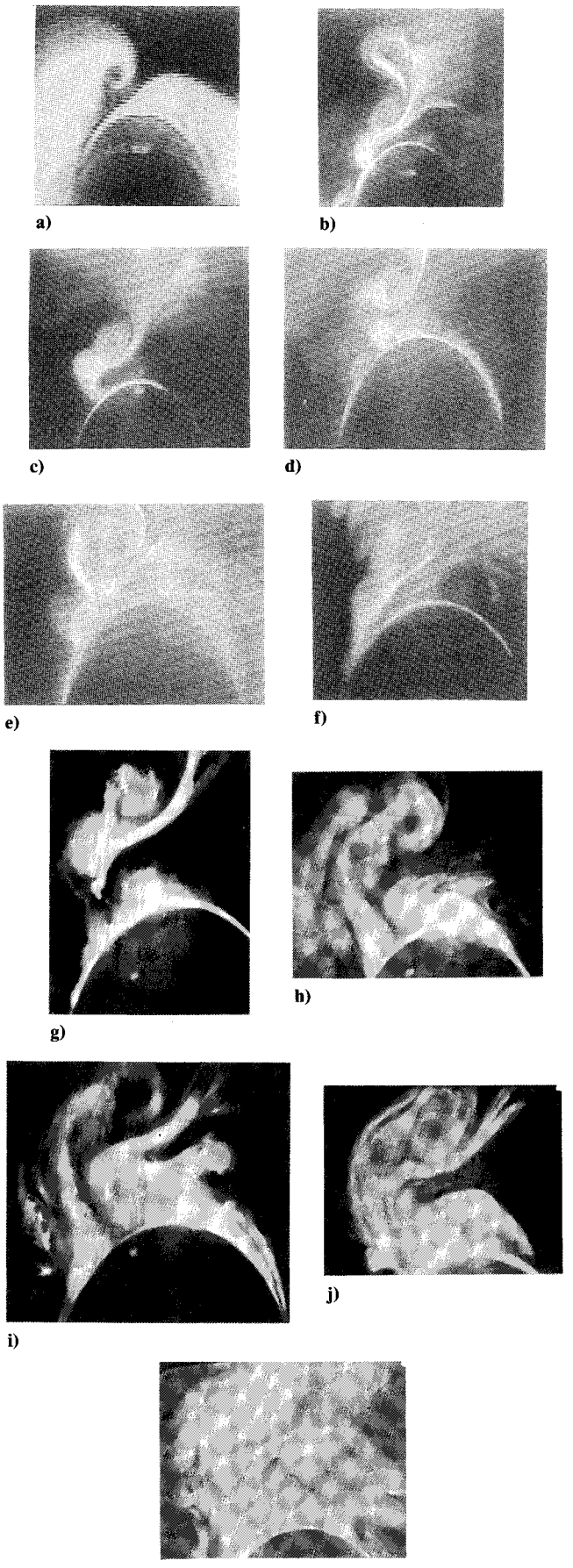

Fig. 5 A series of sample photographs of the lee flow structure at: a) $X/D=0.3$; b) $X/D=0.5$; c) $X/D=0.6$; d) $X/D=0.7$; e) $X/D=0.8$; f) $X/D=0.9$; g) $X/D=1.5$; h) $X/D=1.6$; i) $X/D=1.7$; j) $X/D=1.8$; and k) $X/D=2.0$.

to the leeward meridian. No inflection point is visible on the left-hand side of the model in these sections, although the flow-visualization experiment has shown clearly that boundary-layer separation occurs close to a lateral angle of 90 deg. In all three cases, the differences in pressure, between the right and the left sides, do not result in significant side forces.

The pressure distributions on the two sides of the model become quite different as the incidence angle is increased to 45 deg, particularly at $X/D=0.9$. Farther downstream, the minimum values of C_p on the right-hand side increase, whereas the corresponding values on the left-hand side decrease. Note, that the pressure distribution at $X/D=0.9$ results in a large side force to the right, and the results at $X/D=2.9$ indicate a small side load to the left. The latter, "almost" symmetric distribution, obviously does not indicate a flow structure even close to being symmetric. By following the topologies, however, one can observe that the primary attachment point (sepa-

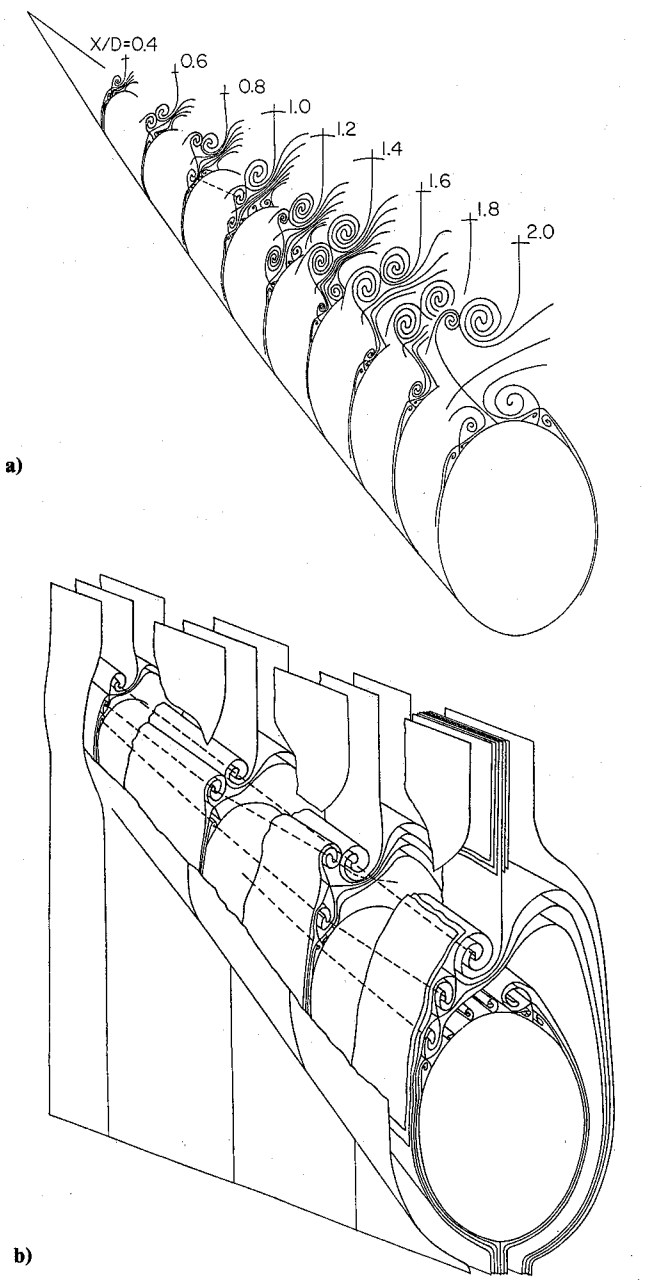

Fig. 6 Three-dimensional sketches showing the stream surfaces associated with the left-hand primary structures. The focus is on entrainment of growing secondary structures by the original left primary nodes (for simplicity most of the secondary structures are omitted).

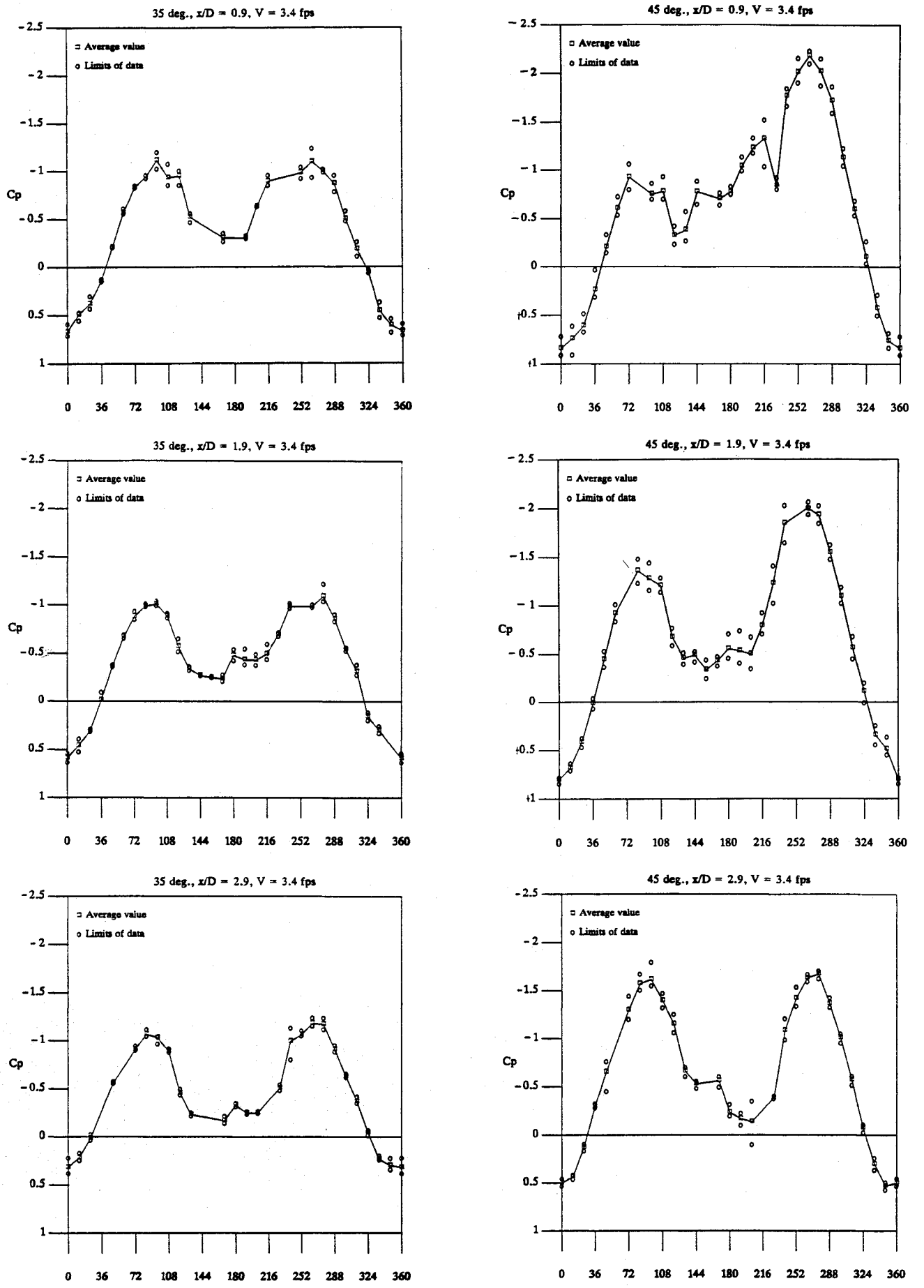

Fig. 7 The pressure-coefficient distribution around an inclined 3.5*l*/*D* ogive. 0 deg is the windward meridian and 180 deg is the leeward meridian. *x* is the axial distance from the tip. The angle increases in a clockwise direction.

rating the structures originated on the left side from those generated on the right side of the model) moves from about 140 deg at $X/D=0.9$ to 165 deg at $X/D=2.0$, and to about 185 deg at $X/D=3.0$. Thus, one should expect a more "symmetric" pressure at $X/D=2.9$, and a change in the direction of the side force. The existence of a large side force as early as $X/D=0.9$, its reduction and reversal already at $X/D=2.9$, does not agree with the results of Lamont,[19] for example, who measured peak side forces at much higher values of X/D. The reason for the discrepancy cannot be explained without some speculation. It may be a result of a different Reynolds number (observe the changes in Lamont's results for the same body when the Re_D is tripled from 4×10^5 to 1.25×10^6 at 40-deg incidence), incidence angle (see Ref. 16 for a comparison between 40 and 45 deg on the same model), freestream turbulence etc. The present distributions at 45 deg, however, do resemble qualitatively the transitional distributions in Lamont's results.

An attempt to compare the pressure distributions to the flow topologies results only in partial success. The difficulties in interpreting the data are related primarily to the complexity of the wake structure close to the surface. (Note also that the pressure was measured at the same axial section, while the visualization planes are perpendicular to the direction of motion.) At $X/D=0.9$ and 45-deg incidence, the inflection point close to 90 deg agrees with the location of boundary-layer separation. However, the recovery beyond 180 deg cannot be explained without some speculations. The impingement on the surface of the fluid arriving from the right-hand side, which is evident in the topology of $X/D=1.0$, is a possible explanation. Close to 144 deg the pressure decreases again, *maybe* due to the proximity of the large left primary nodes (see also Figs. 3 and 5 for sample photographs). The right-hand side (still at $X/D=0.9$) contains two pressure minima. The first one is located 264 deg, and the second at 216 deg. The latter is probably related to the existence of the right primary structure, even though it is located slightly to the right (higher lateral angle) of the focus. The narrow region separating these two minima (216 and 264 deg) is located under the secondary structures of the righ-hand side (see Fig. 2).

At $X/D=1.9$, there are clearly two secondary dips, the first around 144 deg and the second close to 180 deg. From Fig. 2 and the last photograph of Fig. 5, it is clear that these dips match with the location of the larger foci of coalescing stream surface which are located close to the surface. The increasing distance of the detached nodes from the model may be responsible for the reduction in their influence on the pressure distribution. Note that at this location there is only one pressure minimum on the right-hand side. We cannot provide a convincing explanation for the reduction in the magnitude of the pressure peak associated, presumably, with the right primary structure (compare the peak at $X/D=0.9$ at 216 deg to the peak at $X/D=1.9$ at 180 deg). It may be a result of the initial stages of detachment of the right-hand primary center. At $X/D=2.9$, there is only a single visible secondary peak close to 168 deg. The last topology sketch in Fig. 2 demonstrating the existence of a single, large, clockwise-rotating center close to the surface may be an explanation for this peak.

In general, pressure measurements every 12 deg, such as the present data, are too crudely spaced to be able to identify the effects of the secondary structure. As a result, the correlations between the flow topologies (flow visualizaton) and the pressure distributions are not completely conclusive, and leave a lot of room for speculation. If one wishes to resolve the pressure changes associated with the smaller centers, the spaces between pressure taps, particularly close to the separation point must be reduced to within 2 deg.

Summary and Conclusions

The results of a series of flow-visualization experiments are used for sketching the topology of the flow structures in the lee of an inclined body of revolution. Several phenomena are demonstrated by the topologies. The most obvious is that the asymmetric flow structure (at the particular incidence angle, 45 deg, and Reynolds number, 2.7×10^5) is dominated by multiple, and continuously generated, secondary centers of coalescing stream surfaces. The process starts when the left primary nodes starts detaching from the surface. The secondary structure rotating in the same direction just below it also "moves" away from the surface while growing in size. A new pair of secondary structures then forms in the vacated space. Farther downstream the two detached centers interlace around each other, until the original primary focus entrains the enlarged secondary structure. Once this process is completed, a new secondary focus starts growing, detaches from the surface, and is eventually entrained into the original primary center. During the preliminary stages of asymmetry, the right primary center moves toward the leeward meridian. The detachment of the clockwise-rotating structure also leaves a series of closely spaced secondary structures, located close to the surface with counterclockwise-rotating fluid. These nodes are eventually entrained into the right primary center. Once the condition defined as a complete detachment of the primary left focus occurs, it becomes enclosed in a separate "shell" of stream surfaces and does not entrain additional fluid originated from the model's boundary layer. At this stage, the right primary center starts lifting away from the surface and a new cycle starts. A pair of overall views of the lee flow structure is also plotted by superimposing a number of the topology plots into two three-dimensional images. These sketches focus on the development and eventual entrainment of the secondary structures on the left-hand side of the model.

The present paper also includes the results of surface pressure measurements at 35 and 45 deg. At the lower angle the flow structure, as well as the surface pressure distribution, are slightly asymmetric. At 45 deg, the pressure distributions display a reversal of the side forces. At $X/D=0.9$ and 1.9, the side force is to the right, whereas at $X/D=2.9$, it changes its direction to the left. Only a crude correlation can be made between the surface pressure and the flow topologies. It seems that the dominating factor in determining the direction of the side force is the proximity of the primary centers. When the left structure starts lifting away from the surface and the right focus moves closer to the surface, the pressure is lower on the right-hand side. When the right center starts detaching, the side force is reversed due to the reduction in pressure associated with the proximity of the large left focus.

Acknowledgment

This work was supported in part by the National Science Foundation and in part by the Office of Naval Research Applied Hydrodynamics Research Program.

References

[1]Allen, H. J. and Perkins, E. W., "Characterisitcs of Flow Over Inclined Bodies of Revolution," NACA RM A50L07, 1951.

[2]Keener, E. R. and Chapman, G. T., "Onset of Aerodynamic Side Forces at Zero Sideslip on Symmetric Forebodies at High Angles of Attack," AIAA Paper 74-0770, 1974.

[3]Lamont, P. J. and Hunt B. L., "Pressure and Force Distributions on a Sharp-Nosed Circular Cylinder at Large Angles of Inclination to a Uniform Subsonic Stream," *Journal of Fluid Mechanics,* Vol. 76, 1976, pp. 519-559.

[4]Lamont, P. J., "The Complex Asymmetric Flow Over a 3.50 Ogive Nose and Cylindrical Afterbody at High Angles of Attack," AIAA Paper 82-0053, Jan. 1982.

[5]Pick, G. S., "Investigation of Side Force on Ogive-Cylinder Bodies at High Angles of Attack in the $M=0.5$ to 1.1 Range," AIAA Paper 71-0570, 1971.

[6]Thomson, K D. and Morrison, D. F., "The Spacing, Position, and Strength of Vortices in the Wake of Slinder Cylindrical Bodies at Large Incidence," *Journal of Fluid Mechanics,* Vol. 50, No. 4, 1971, pp. 751-783.

[7]Keener, E. R., "Oil-Flow Separtion Patterns on an Ogive Forebody," NASA TM-81314, Oct. 1981.

[8]Peake, D. J. and Tobak, M., "Three-Dimensional Interactions and Vortical Flows with Emphasis on High Speeds," AGARD-AG-252, July 1980.

[9]Yanta, W. J. and Wardlaw, A. B., "Laser Doppler Velocimeter Measurements of Leeward Flowfields on Slender Bodies at Large Angles of Attack," AIAA Paper 77-0660, 1977.

[10]Wardlaw, A. B. and Yanta, W. J., "Asymmetric Flowfield Development on a Slender Body at High Incidence," *AIAA Journal,* Vol. 2, Feb. 1984, pp. 242–249.

[11]Newsome, R. W. and Kandil, O. A., "Vortical Flow Aerodynamics—Physical Aspects and Numerical Simulation," AIAA Paper 87-0205, Jan. 1987.

[12]Hall, R. M., "Forebody and Missile Side Forces and the Time Analogy," AIAA Paper 87-0327, Jan. 1987.

[13]Ericsson, L. E. and Reding J. P., "Asymmetric Vortex Shedding from Bodies of Revolution," *Tactical Missile Aerodynamics,* Vol. 104, Progress Astro and Aero Series, edited by M. J. Hemsch and J. N. Nielson, AIAA, New York, 1986, Chap. VII, pp. 243–296.

[14]Hunt, B. J., "Asymmetric Vortex Forces and Wakes on Slender Bodies," AIAA Paper 82-1336, Aug. 1982.

[15]Tobak, M. and Peake, D. J., "Topology of Two-Dimensional and Three-Dimensional Separated Flows," AIAA Paper 79-1480, July 1979.

[16]Ward, K. C. and Katz, J., "Development of Structures in the Lee of an Inclined Body of Revolution," *Journal of Aircraft,* Vol. 26, March 1988, pp. 198–206.

[17]Ward, K. C. and Katz, J., "Topology of the Flow Structures Behind an Inclined Projectile: Part A," *Journal of Aircraft,* Vol. 26, Nov. 1989, pp. 1016–1022.

[18]Bueno-Galdo, J. and Katz, J., "The Effects of Surface Roughness on the Roll-up Process of a Tip Vortices on a Rectangular Hydrofoil," AIAA Paper 88-3744, June 1988.

[19]Lamont, P. J., "The Effect of Reynolds Number on Normal and Side Forces on Ogive-Cylinder At High Incidence," AIAA Paper 85-1799.